PCCP

Accepted Manuscript

ROYAL SOCIETY OF CHEMISTRY

www.rsc.org/pccp

Journal Name

ARTICLE TYPE

Cite this: DOI: 10.1039/xxxxxxxxxx

Tuning Oxide Activity through Modification of the Crystal and Electronic Structure: From Strain to Potential Polymorphs†

Zhongnan Xu,[a] John R. Kitchin,*[a]

Received Date
Accepted Date

DOI: 10.1039/xxxxxxxxxx

www.rsc.org/journalname

Discovering new materials with tailored chemical properties is vital for advancing key technologies in catalysis and energy conversion. One strategy is the modification of a material's crystal structure, and new methods allow for the synthesis and stabilization of potential materials in a range of crystal polymorph structures. We assess the potential reactivity of four metastable oxide polymorphs of MO_2 (M=Ru, Rh, Pt, Ir) transition metal oxides. In spite of the similar local geometry and coordination between atoms in the metastable polymorphic and stable rutile structure, we find that polymorph reactivities cannot be explained by strain alone and offer tunable reactivity and increased stability. Atom-projected density of states reveals that the unique reactivity of polymorphs are caused by a redistribution of energy levels of the t_{2g}-states. This structure-activity relationship is induced by slight distortions to the M-O bonds in polymorphic structures and is unattainable by strain. We predict columbite IrO_2 to be more active than rutile IrO_2 for oxygen evolution.

1 Introduction

The discovery of new materials with tailored chemical properties is vital for advancing key technologies related to catalysis and energy conversion[1,2]. Transition metal oxides (TMOs) catalyze a number of these key technologies, including water electrolysis, fuel cells, and photocatalysis[3–5]. Compared to modifying the composition of TMOs, the search for novel structures for catalytic applications is relatively unexplored. The impact of the crystal structure on catalytic activity is often difficult to pinpoint experimentally. For oxygen evolution, slight changes to bond lengths/angles of amorphous materials result in orders of magnitude differences in activity, but these distortions are accompanied by significant changes in the oxidation state and oxygen vacancy concentration[6–8]. In another example, a recent study found that the symmetric coordination of oxygen around the B ions in a mixed Pt doped $BaCeO_3$ perovskite was key to high water-gas shift (WGS) activity, and oxygen vacancy induced distortions to this symmetry lowered WGS activity[9]. Elucidation of these structure-function relationships would allow for the targeted synthesis of materials with optimized crystal structures.

Polymorph engineering is one potential route to structurally tune the activity of materials. Experimental studies have observed that some metastable polymorphs can lead to significant improvements in catalytic reactions. Multiple polymorphs of Al_2O_3 are stable in reactive conditions and display different support effects[10,11]. Anatase TiO_2 is more photocatalytically active than rutile TiO_2[12]. The structural sensitivity towards formaldehyde and water oxidation has been observed in a number studies including manganese and cobalt oxide polymorphs[7,13–16]. Traditionally, variation of temperature and/or pressure during synthesis can lead to crystallization of different polymorphic structures[17–19]. However, new strategies have proven to be effective at realizing metastable phases. Thin films of metastable polymorphs can be stabilized epitaxially if grown on an appropriate substrate[20,21]. It has been shown that thin films are stable and active towards photocatalysis and oxygen reduction[22–25]. Changing the composition of materials has also been shown to be effective at producing metastable phases, especially when the constituent materials have different ground state structures[26–28]. There are multiple

[a]Department of Chemical Engineering, Carnegie Mellon University, 5000 Forbes Ave., Pittsburgh, Pennsylvania 15213 USA. E-mail: jkitchin@andrew.cmu.edu

† Electronic Supplementary Information (ESI) available: [details of any supplementary information available should be included here]. See DOI: 10.1039/b000000x/

mechanisms of metastable phase stabilization on the nanoscale. The increase in the surface to bulk ratio can stabilize certain metastable phases if surface energies of metastable phases are preferred over stable ones[29]. A recent study reported nucleation of a new phase at the catalyst/nanowire interface during vapor-liquid-solid growth[30].

Given the large number of potential structural polymorphs that are possible, experimental synthesis would be aided by *a priori* information on what polymorphs are possible and desirable to synthesize. Simple comparisons of calculated free energies using density functional theory (DFT) combined with automatic crystal structure generation can build large databases of relative stabilities that quickly direct what might be possible for synthesis[31–33]. Recent DFT studies have also evaluated electronic and physical properties of potential polymorphs as well[34–37]. While a few studies have evaluated surface activity of existing polymorphs[38,39], we are unaware of any studies that have evaluated chemical properties of *potential undiscovered* polymorphs.

In this contribution, we assess the reactivity and stability of four potential oxide polymorphs (anatase, brookite, columbite, pyrite) of MO_2 (M=Ru, Rh, Pt, Ir) transition metal oxides (TMOs), which all form in a rutile-like structure at typical synthesis and reactive conditions. The similar coordination and local geometry of both cations and anions in all structures lead us to hypothesize that strain alone could describe trends in chemical properties of metastable polymorphs. Our results suggest this is not the case. In addition, we observe polymorphic structures provide more tunable reactivity and increased stability with respect to strained rutile structures. Our prediction that columbite IrO_2 will be a better oxygen evolution catalyst than rutile IrO_2 underscores the potential activity benefits of polymorphic structure. The origin of the unique reactivity of polymorphic structures is unearthed through analysis of the electronic structure. In contrast to simple strain, distortions to the octahedral symmetry of the metal cation in polymorphic structures lead to significant changes in both the shape of the t_{2g}-band and adsorption energy.

2 Computational Methods

All calculations were performed using the Vienna Ab-initio Simulation Package (VASP)[40,41] with the Perdew-Burke-Ernzerhof (PBE)[42,43] generalized gradient approximation (GGA) exchange-correlation functional. The core electrons were were described by the projector augmented-wave (PAW) method[44,45]. The Kohn-Sham orbitals were expanded with plane-waves up to a 500 eV cutoff. All k-points were represented on Monkhorst-Pack grids[46]. System specific k-point grids, force convergence, and additional calculation parameters can be found in the supporting information.

The two primary chemical properties we calculated in this study are oxygen adsorption and vacancy formation energies. Using DFT computed total energy values, the formulas for both quantities are shown below.

$$\Delta E^{O}_{ads} = E_{slab,O} - E_{slab} - \frac{E_{O_2}}{2} \quad (1)$$

$$\Delta E^{O}_{vac} = E_{bulk,vac} + \frac{E_{O_2}}{2} - E_{bulk,stoic} \quad (2)$$

$E_{slab,O}$ and E_{slab} are the total energies of an oxide slab with and without an adsorbed oxygen atom, respectively. $E_{bulk,stoic}$ and $E_{bulk,vac}$ are the total energies a bulk oxide with and without an oxygen vacancy. All vacancy formation energies were calculated at a 6.25% vacancy concentration. Free energies of adsorption energies of OER intermediates were calculated using the atomistic thermodynamic framework and zero-point corrections employed in previous work[47,48].

3 Results and Discussion

The compounds we model in this study are four late transition metal dioxides of RuO_2, RhO_2, IrO_2, and PtO_2, which are used in a number of industrially relevant technologies[49,50]. Ruthenium and iridium oxides are known to be the most active oxygen evolution catalysts[50]. Rhodium and platinum oxides are active for NO reduction[51] and syngas production[52,53]. The activity of a catalyst in these applications is often related a few key intermediate's adsorption energy, which is one of the primary chemical properties we evaluate in this study[48,54].

In addition to their stable rutile phase, we also model possible polymorphs of anatase, brookite, columbite, and pyrite (Figure 1). Of these compound/phase pairs, only a few have been experimentally observed. RuO_2 has been observed in the pyrite-type phase at high pressure[55,56]. A recent study correctly predicted the possibility of this polymorph using DFT and further proposed columbite and pyrite as possible synthesis targets of IrO_2 and RuO_2[57]. Rutile-like β-PtO_2 is one of the three stable experimentally observed polymorphs of PtO_2, though the structures modeled in this study have not be observed. RhO_2 has only been experimentally observed in a rutile like structure[58].

In addition to being potential undiscovered synthesis targets, these polymorphs also allow us to isolate the effect structural distortions have on catalytic activity. Inspection of all crystal structures considered in this study reveals a similar octahedral coordination with six M-O bonds to all metal cations (Figure 1). Furthermore, all oxygen ions have a trigonal planar-like coordination, forming three O-M bonds for each oxygen anion. Hence, the local environment of both the cation and anion is similar across all structures, and all differences between polymorphs lie in structural distortions of bond lengths and angles. These distortions to the octahedral are similar to those observed by EXAFS in a number of experiments relating a distorted structure and different ac-

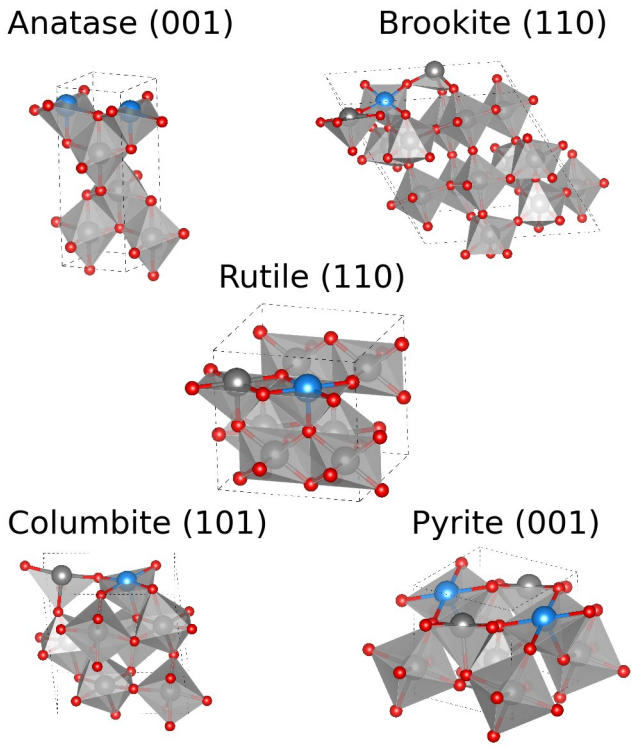

Fig. 1 In addition to the stable rutile phase, the four metastable polymorphs used in this study. Images show the octahedral coordination present for metal cations found in all structures, along with the 5cus site used for all adsorption energy calculations. The periodic cell shown is the unit cell required for the construction of each specific surface.

tivity of TMOs for a number of reactions[6,59–61].

We want to determine the effect these polymorph-induced distortions have on their reactivity. We do this by calculating both oxygen adsorption and vacancy formation energies. Vacancy formation energies are calculated in the bulk at the same vacancy concentration. While different crystal structures naturally produce a large number of different adsorption sites through geometrically different surface facets, this analysis is not our focus. It is already well known that differences in coordination or stoichiometry of the surface adsorption site can produce significant differences in adsorption behavior. Our objective is to evaluate the effect that distortions to the MO_6 geometry have on the adsorption energy. To isolate the effect of distorting the MO_6 octahedral on the adsorption energy, we choose adsorption sites on M ions with the same number of missing bonds that maximizes the number of surface and sub-surface M-O bonds. This happens to be the 5cus site. The facets we model that capture similar 5cus sites are shown in Figure 1, and DFT studies show some of these surface facets are predicted to be thermodynamically stable[62–64]. Note we could not find a study on relative surface stabilities of the columbite structure, but our calculations show no major surface reconstructions on the columbite (101) surface. Details on the construction of these surfaces can be found in the supporting information. All adsorption calculations were calculated on these surfaces at the adsorption site shown in Figure 1.

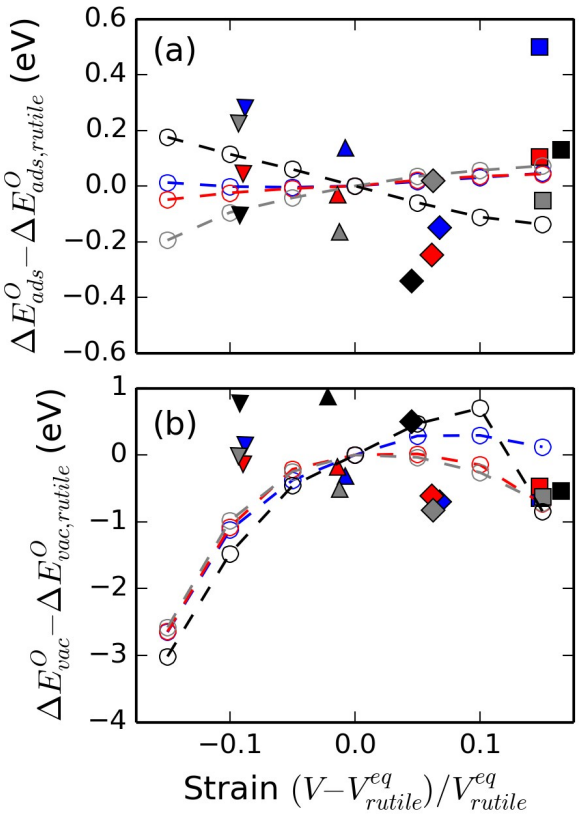

Fig. 2 (a) Adsorption and (b) vacancy formation energies of all polymorphs and strained rutile plotted against the strain relative to the equilibrium volume of rutile of each respective element. Rutile is given by open ◯ and the dashed lines connects rutile structures with different amounts of isotropic strain. Anatase, brookite, columbite, and pyrite are given by □, ▽, △, and ◇ markers, respectively. RuO_2, RhO_2, IrO_2, and PtO_2 given by gray, red, blue, and black colored markers, respectively.

The similar MO_6 environment of both the metal and oxygen ion in all crystal structures leads us to hypothesize that the M-O bond lengths should correlate with chemical properties. Differences in the M-O bond lengths between different crystal structures – or strain – should express itself as differences in the volume. Hence, in this study we define the strain of a specific MO_2-polymorph as the difference of its volume with the equilibrium volume of rutile MO_2. Correlations between strain and adsorption and vacancy energies have been observed in a number of DFT studies[65,66]. Figure 2 validates these correlations for rutile, showing smooth

strain-dependent ΔE^O_{ads} and ΔE^O_{vac}. Surprisingly, adsorption on metastable polymorphs do not fall on these correlations. In addition, the changes in the adsorption energy caused by changing the crystal structure is oftentimes higher in magnitude then changes caused by straining rutile.

In contrast to adsorption energies, applying strain to rutile produces a much larger change in ΔE^O_{vac} than altering its crystal structure. Applying either compressive or tensile strain results in more exothermic vacancy formation, and ΔE^O_{vac} in polymorphs tend to be more endothermic than highly strained rutile. These results can be understood through structure stability. Straining rutile causes structural instability and allows for a greater degree of relaxation when a vacancy is created. This structural instability is also evident in strain-induced crystal phase transitions [67,68]. In contrast, polymorph structures, which are fully relaxed at their equilibrium volume, are more resistant to vacancy formation. This conclusion has important implications on the stability of these structures. A polymorph, though globally metastable, should have comparable stability in reactive environments where oxygen vacancies are regularly being created/filled. This result is consistent with studies where metastable structures were found to be stable in reactive conditions and showed structural-sensitive activity [13,14,16].

Correlations between adsorption energies and vacancy formation energies have been observed in past research and have ramifications on the balance of activity and stability of oxide materials [65,69,70]. In Figure 3 (a), we also find correlations between adsorption and vacancy formation in the context of strain on rutile, but polymorphs do not follow these correlations. Furthermore, polymorphs exhibit a much larger degree of tunability of its adsorption energy without sacrificing stability. This observation motivates the search for polymorphs as possible candidates for breaking typical activity/stability trade-offs in catalytic operations.

To assess the potential catalytic activity of oxide polymorphs, we calculate adsorption energies O, OH, and OOH with respect to the standard hydrogen electrode (SHE). Using a previously established atomistic thermodynamic framework, adsorption energies of O, OH, and OOH can predict the OER activity of catalysts [47,48]. Consistent with previous results, in Figure 3 (b) we find that adsorption energies of O, OH, and OOH scale with each other, and adsorption energies on polymorphs fall on the same scaling as that of the rutile structures. We suspect this scaling persists due to the similar geometric structure of the adsorption site, which has been observed to be a requirement on metal surfaces [71,72]. Figure 3 (b) further demonstrates using structural sensitivity to tune adsorption energies, where adsorption energies between those on stable rutile structures of different compounds are realized on polymorph structures.

The polymorph's ability to adjust adsorption energies along

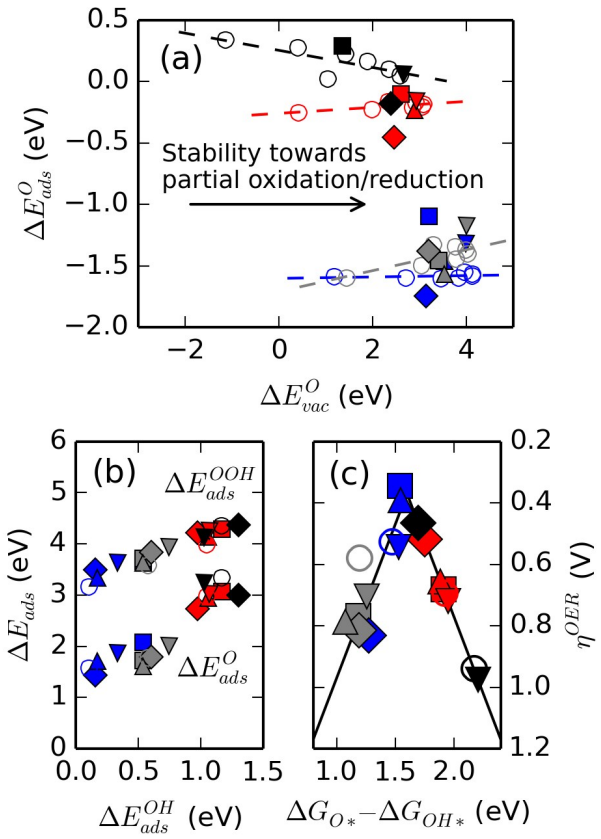

Fig. 3 (a) Correlation between the adsorption and vacancy formation energy of all structures. (b) Scaling relationships between adsorption energies on O, OH, and OOH for all systems. (c) Theoretical overpotential towards oxygen evolution of all compounds. Rutile is given by open ◯ and the dashed lines connects rutile structures with different amounts of isotropic strain. Anatase, brookite, columbite, and pyrite are given by □, ▽, △, and ◇ markers, respectively. RuO_2, RhO_2, IrO_2, and PtO_2 given by gray, red, blue, and black colored markers, respectively.

scaling relationships imply their activities should fall on the OER activity volcano and potentially give different activities with respect to rutile [48]. This is shown in Figure 3 (c). Anatase and columbite IrO_2 and brookite RhO_2 and PtO_2 are predicted to be more active than their stable rutile forms. Work in our group suggest columbite IrO_2 as a potential synthesis target through thin film growth [57]. Our results further motivate the experimental efforts in the synthesis of columbite IrO_2.

While late transition metal oxide structures of anatase and brookite have been calculated to be high in energy and unfeasible to synthesize directly via either high pressure or thin film growth, TiO_2 is naturally occuring in both of these structures, easily synthesized, and stable under electrochemical and photochemical conditions [73,74]. Futhermore, anatase and brookite TiO_2

have heightened photocatalytic activity and rutile TiO_2 can incorporate a large variety of transition metals as dopants[75]. We therefore hypothesize Pt and Rh doped TiO_2 brookite or Ir doped TiO_2 anatase should increase photocatalytic water oxidation activity.

We stress again that the primary point of our OER analysis to assess whether from a computational standpoint, we expect the structural distortions induced by polymorphs can produce significant changes in activity. We could have chosen any reaction for this test, but we choose OER due to the efficacy and simplicity of previously established models for evaluating catalytic activity[48,76,77] and the usage of RuO_2 and IrO_2 as state of the art OER catalysts. Our results motivate a more in-depth evaluation of the stability and activity of columbite IrO_2, which includes the stability of several surface facets/terminations, activity of multiple adsorption sites, and a full potential energy landscape analysis.

Having demonstrated the unique activity and stability offered by potential polymorphs, we now investigate the origin of these properties by analyzing both the atomic and electronic structure. The case study we perfrom to elucidate these structure-property relationships is IrO_2 in rutile, strained rutile, and columbite crystal structures. Figure 2 shows that rutile and columbite have similar equilibrium volumes and visualization of their crystal structures reveal a similar hcp lattice of oxygen. Despite these similarities, changing the crystal structure from rutile to columbite produces a $\sim$0.15 eV change in adsorption energy, while straining IrO_2 has neglible effects on adsorption.

Table 1 Bond lengths and angles of strained rutile IrO_2 and columbite at the adsorption site. IrO_2^R, $IrO_2^{R+0.15}$, $IrO_2^{R-0.15}$, IrO_2^C refer to IrO_2 in the equilibrium rutile phase, rutile with 15% tensile strain, 15% compressive strain, and the columbite phase. $l_{M-O^{sub}}$ and $l_{M-O^{surf}_{i=1,2,3,4}}$ refer to bond lengths of the metal cation at the adsorption site with the single sub-surface and four surface oxygen anions, respectively. $\theta_{O_i^{surf}-M-O_j^{surf}}$ refers to the angle formed between two surface oxygen atoms and the metal cation at the adsorption site.

System	IrO_2^R	$IrO_2^{R+0.15}$	$IrO_2^{R-0.15}$	IrO_2^C
$l_{M-O^{sub}}$ (Å)	1.950	2.102	1.865	2.028
$l_{M-O_1^{surf}}$ (Å)	2.012	2.090	1.926	2.061
$l_{M-O_2^{surf}}$ (Å)	2.012	2.090	1.926	1.913
$l_{M-O_3^{surf}}$ (Å)	2.012	2.090	1.926	1.965
$l_{M-O_4^{surf}}$ (Å)	2.012	2.090	1.926	1.893
$\theta_{O_1^{surf}-M-O_2^{surf}}$	74.6	76.9	72.1	97.5
$\theta_{O_2^{surf}-M-O_3^{surf}}$	104.9	103.1	107.9	84.3
$\theta_{O_3^{surf}-M-O_4^{surf}}$	74.6	76.9	72.1	89.8
$\theta_{O_4^{surf}-M-O_1^{surf}}$	104.9	103.1	107.9	88.1

Analysis of the atomic structure gives some insight into this effect. Table 1 shows the bond lengths and angles of Ir at the adsorption site on the rutile (110) and columbite (101) surface. Applying strain to rutile does not the break the original symmetry around the adsorption site, and no significant change of bond angles is observed of any rutile structures. Furthermore, strain induced bond length changes are not as high relative to the volume change, which is due to internal relaxations that reduce the effect of strain. In contrast, the columbite octahedral contains distortions relative to the octahedral found in the rutile crystal structure.

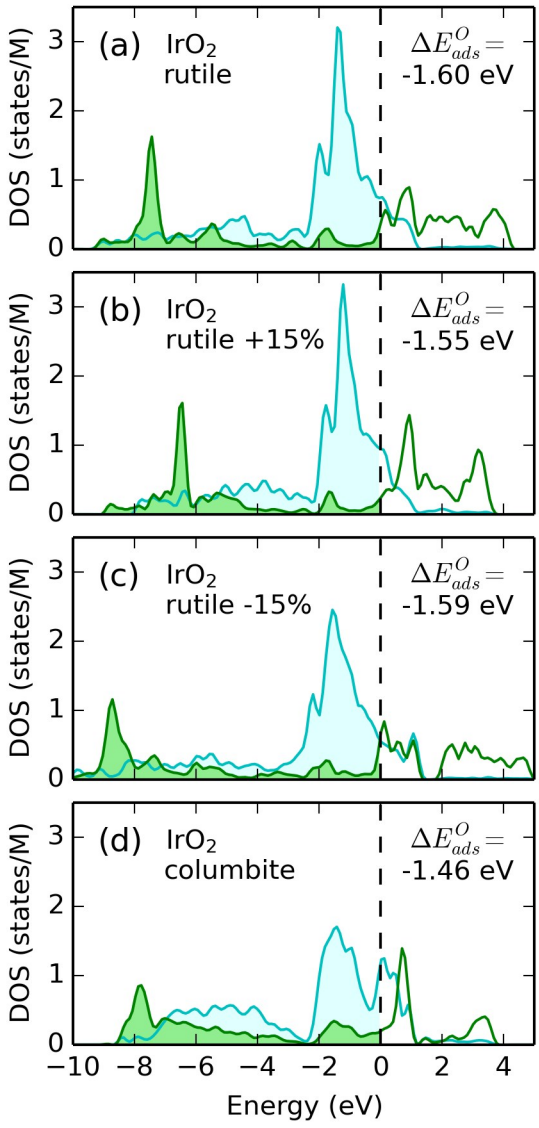

Fig. 4 Density of states of rutile IrO_2, rutile with maximum tensile and compressive strain. The green area represents the e_g states, and the cyan area represent the t_{2g} states. Filled areas represent the occupied electronic states below the Fermi level.

The effect these structural changes have on the adsorption en-

ergy can be seen in the electronic structure. Figure 4 shows the atomic projected density of states of Ir at the adsorption site in rutile, strained rutile, and columbite IrO_2. The striking feature that persists for all rutile structures is the shape and position of the t_{2g}-bands near the Fermi level, while the e_g-band undergoes significant changes to both the shape and positions upon strain. In contrast, the t_{2g}-band shape and position is significantly different for Ir in the columbite crystal structure when compared to any rutile DOS. IrO_2 columbite e_g-band has its low energy bonding and high energy anti-bonding orbitals at similar energy levels to IrO_2 rutile. Similar conclusions can be found for a majority of all other systems in this study, and all DOS data can be found in the supporting information.

Our two conclusions from the analysis of the changes in adsorption energy, atomic structure, and electronic structure in this case study are as follows: (1) the shape and position of the t_{2g}-states is vital for determining the strength of adsorption, and (2) distortions to M-O bonds within the octahedral geometry results in redistribution of the t_{2g}-band. Both of these conclusions are surprising. Considering that the e_g-orbitals make σ-bonds with surface and adsorbate oxygen p-orbitals[78], the energy levels of the e_g-orbitals should determine the bond strength. Likewise, distortions to the M-O bonds should express themselves as changes to the shape and energy levels of the e_g-bands. Our results show otherwise but are consistent with recent work that show trends in adsorption energies can be correlated to the center of t_{2g}-states near the fermi level[66,79]. While universal correlations between properties of the electronic structure and the adsorption energy could not be found in this study, we suspect the higher ΔE^O_{ads} on columbite IrO_2 with respect to rutile IrO_2 come from the creation of high energy t_{2g} states at the Fermi level. Because these states are degenerate in energy with anti-bonding e_g-band, they are likely repulsive and serve to destabilize surface-adsorbate bond.

4 Conclusions

In light of the growing interest and ability to search structural space for new materials, we have explored the chemical properties of potential oxide polymorphs. We find that changes to adsorption and vacancy formation energies on polymorph structures cannot be explained by strain alone, allowing greater tunability in their adsorption properties while maintaining stability in reactive environments. We highlight this tunability by predicting certain polymorphs such as columbite IrO_2 to be more active for oxygen evolution and discuss their possible implementation. Analysis of both the atomic and electronic structure reveal distortions to the MO_6 octahedral geometry imparted through polymorphic structures cause significant redistribution of energy levels of the t_{2g}-states. Coupled with calculated adsorption energies, our results emphasize the key role the t_{2g}-states in determining the strength of adsorption.

References

1 J. K. Nørskov and T. Bligaard, *Angew. Chem. Int. Edit.*, 2013, **52**, 776–777.

2 A. Jain, S. P. Ong, G. Hautier, W. Chen, W. D. Richards, S. Dacek, S. Cholia, D. Gunter, D. Skinner, G. Ceder and K. A. Persson, *APL Mat.*, 2013, **1**, 011002.

3 N. Q. Minh, *J. Am. Ceram. Soc.*, 1993, **76**, 563–588.

4 M. R. Hoffmann, S. T. Martin, W. Choi and D. W. Bahnemann, *Chem. Rev.*, 1995, **95**, 69–96.

5 S. Trasatti, *Electrochim. Acta*, 2000, **45**, 2377–2385.

6 D. K. Bediako, B. Lassalle-Kaiser, Y. Surendranath, J. Yano, V. K. Yachandra and D. G. Nocera, *J. Am. Chem. Soc.*, 2012, **134**, 6801–6809.

7 A. Bergmann, I. Zaharieva, H. Dau and P. Strasser, *Energy Environ. Sci.*, 2013, **6**, 2745–2755.

8 D. González-Flores, I. Sánchez, I. Zaharieva, K. Klingan, J. Heidkamp, P. Chernev, P. W. Menezes, M. Driess, H. Dau and M. L. Montero, *Angew. Chem. Int. Edit.*, 2015, **127**, 2502–2506.

9 T. Rajesh and R. N. Devi, *J. Phys. Chem. C*, 2014, **118**, 20867–20874.

10 M. A. Trunov, M. Schoenitz, X. Zhu and E. L. Dreizin, *Combust. Flame*, 2005, **140**, 310–318.

11 J. J. H. B. Sattler, J. Ruiz-Martinez, E. Santillan-Jimenez and B. M. Weckhuysen, *Chem. Rev.*, 2014, **114**, 10613–10653.

12 H. G. Yang, C. H. Sun, S. Z. Qiao, J. Zou, G. Liu, S. C. Smith, H. M. Cheng and G. Q. Lu, *Nature*, 2008, **453**, 638–641.

13 G. P. Gardner, Y. B. Go, D. M. Robinson, P. F. Smith, J. Hadermann, A. Abakumov, M. Greenblatt and G. C. Dismukes, *Angew. Chem. Int. Edit.*, 2012, **51**, 1616–1619.

14 D. M. Robinson, Y. B. Go, M. Mui, G. Gardner, Z. Zhang, D. Mastrogiovanni, E. Garfunkel, J. Li, M. Greenblatt and G. C. Dismukes, *J. Am. Chem. Soc.*, 2013, **135**, 3494–3501.

15 Y. Meng, W. Song, H. Huang, Z. Ren, S.-Y. Chen and S. L. Suib, *J. Am. Chem. Soc.*, 2014, **136**, 11452–11464.

16 J. Zhang, Y. Li, L. Wang, C. Zhang and H. He, *Catal. Sci. Technol.*, 2015, **5**, 2305–2313.

17 P. Cox, *The Surface Science of Metal Oxides*, Cambridge university press, 1996.

18 S. V. Ovsyannikov, A. M. Abakumov, A. A. Tsirlin, W. Schnelle, R. Egoavil, J. Verbeeck, G. Van Tendeloo, K. V. Glazyrin, M. Hanfland and L. Dubrovinsky, *Angew. Chem. Int. Edit.*, 2013, **52**, 1494–1498.

19 C. M. Pépin, A. Dewaele, G. Geneste, P. Loubeyre and M. Mezouar, *Phys. Rev. Lett.*, 2014, **113**, 265504.

20 P. A. Salvador, T.-D. Doan, B. Mercey and B. Raveau, *Chem. Mater.*, 1998, **10**, 2592–2595.

21 B. Mercey, P. A. Salvador, W. Prellier, T.-D. Doan, J. Wolfman,

M. Hervieu and B. Raveau, *J. Mater. Chem.*, 1999, **9**, 233–242.
22 A. M. Schultz, P. A. Salvador and G. S. Rohrer, *Chem. Commun.*, 2012, **48**, 2012–2014.
23 L. Yan and P. A. Salvador, *ACS Appl. Mater. Interfaces*, 2012, **4**, 2541–2550.
24 D. Lee, A. Grimaud, E. J. Crumlin, K. Mezghani, M. A. Habib, Z. Feng, W. T. Hong, M. D. Biegalski, H. M. Christen and Y. Shao-Horn, *J. Phys. Chem. C*, 2013, **117**, 18789–18795.
25 K. A. Stoerzinger, W. Lü, C. Li, Ariando, T. Venkatesan and Y. Shao-Horn, *J. Phys. Chem. Lett.*, 2015, **6**, 1435–1440.
26 A. Dianat, N. Seriani, M. Bobeth, W. Pompe and L. C. Ciacchi, *J. Phys. Chem. C*, 2008, **112**, 13623–13628.
27 J. Bang, S. Matsuishi, H. Hiraka, F. Fujisaki, T. Otomo, S. Maki, J.-i. Yamaura, R. Kumai, Y. Murakami and H. Hosono, *J. Am. Ceram. Soc.*, 2014, **136**, 7221–7224.
28 R. S. Koster, C. M. Fang, M. Dijkstra, A. van Blaaderen and M. A. van Huis, *J. Phys. Chem. C*, 2015, **119**, 5648–5656.
29 A. Navrotsky, *ChemPhysChem*, 2011, **12**, 2207–2215.
30 J. Gao, O. I. Lebedev, S. Turner, Y. F. Li, Y. H. Lu, Y. P. Feng, P. Boullay, W. Prellier, G. van Tendeloo and T. Wu, *Nano Lett.*, 2012, **12**, 275–280.
31 B. Meredig and C. Wolverton, *Nat. Mater.*, 2013, **12**, 123–127.
32 B. Meredig, A. Agrawal, S. Kirklin, J. E. Saal, J. W. Doak, A. Thompson, K. Zhang, A. Choudhary and C. Wolverton, *Phys. Rev. B*, 2014, **89**, 094104.
33 Y. Wang and Y. Ma, *J. Chem. Phys.*, 2014, **140**, 040901.
34 T. Zhu and S.-P. Gao, *J. Phys. Chem. C*, 2014, **118**, 11385–11396.
35 G. Wachter, C. Lemell, J. Burgdörfer, S. A. Sato, X.-M. Tong and K. Yabana, *Phys. Rev. Lett.*, 2014, **113**, 087401.
36 L. Sponza, J. Goniakowski and C. Noguera, *Phys. Rev. B*, 2015, **91**, 075126.
37 D. Bayerl and E. Kioupakis, *Phys. Rev. B*, 2015, **91**, 165104.
38 S. E. Collins, M. A. Baltanás and A. L. Bonivardi, *Langmuir*, 2005, **21**, 962–970.
39 F. De Angelis, C. Di Valentin, S. Fantacci, A. Vittadini and A. Selloni, *Chem. Rev.*, 2014, **114**, 9708–9753.
40 G. Kresse and J. Furthmüller, *Comp. Mater. Sci.*, 1996, **6**, 15–50.
41 G. Kresse and J. Furthmüller, *Phys. Rev. B*, 1996, **54**, 11169–11186.
42 J. P. Perdew, K. Burke and M. Ernzerhof, *Phys. Rev. Lett.*, 1996, **77**, 3865–3868.
43 J. P. Perdew, K. Burke and M. Ernzerhof, *Phys. Rev. Lett.*, 1997, **78**, 1396–1396.
44 P. E. Blöchl, *Phys. Rev. B*, 1994, **50**, 17953–17979.
45 G. Kresse and D. Joubert, *Phys. Rev. B*, 1999, **59**, 1758–1775.
46 H. J. Monkhorst and J. D. Pack, *Phys. Rev. B*, 1976, **13**, 5188–5192.
47 J. Rossmeisl, Z.-W. Qu, H. Zhu, G.-J. Kroes and J. K. Nørskov, *J. Electroanal. Chem.*, 2007, **607**, 83–89.
48 I. C. Man, H.-Y. Su, F. Calle-Vallejo, H. A. Hansen, J. I. Martínez, N. G. Inoglu, J. Kitchin, T. F. Jaramillo, J. K. Nørskov and J. Rossmeisl, *ChemCatChem*, 2011, **3**, 1159–1165.
49 V. Pârvulescu, P. Grange and B. Delmon, *Catalysis Today*, 1998, **46**, 233–316.
50 C. C. L. McCrory, S. Jung, I. M. Ferrer, S. M. Chatman, J. C. Peters and T. F. Jaramillo, *J. Am. Chem. Soc.*, 2015, **137**, 4347–4357.
51 M. V. Twigg, *Appl. Catal. B-Environ.*, 2007, **70**, 2–15.
52 B. C. Enger, R. Lødeng and A. Holmen, *Appl. Catal. A-Gen.*, 2008, **346**, 1–27.
53 M. Belgued, P. Pareja, A. Amariglio and H. Amarigio, *Nature*, 1991, **352**, 789–790.
54 H. Falsig, T. Bligaard, J. Rass-Hansen, A. L. Kustov, C. H. Christensen and J. K. Nørskov, *Top. Catal.*, 2007, **45**, 117–120.
55 J. Haines, J. M. Léger and O. Schulte, *Science*, 1996, **271**, 629–631.
56 J. S. Tse, D. D. Klug, K. Uehara, Z. Q. Li, J. Haines and J. M. Léger, *Phys. Rev. B*, 2000, **61**, 10029–10034.
57 P. Mehta, P. A. Salvador and J. R. Kitchin, *ACS Appl. Mater. Interfaces*, 2014, **6**, 3630–3639.
58 R. Shannon, *Solid State Commun.*, 1968, **6**, 139–143.
59 M. W. Kanan, J. Yano, Y. Surendranath, M. Dinc˘ a, V. K. Yachandra and D. G. Nocera, *J. Am. Chem. Soc.*, 2010, **132**, 13692–13701.
60 K. Amakawa, L. Sun, C. Guo, M. Hävecker, P. Kube, I. E. Wachs, S. Lwin, A. I. Frenkel, A. Patlolla, K. Hermann, R. Schlögl and A. Trunschke, *Angew. Chem. Int. Edit.*, 2013, **52**, 13553–13557.
61 J. A. Rodriguez, J. C. Hanson, D. Stacchiola and S. D. Senanayake, *Phys. Chem. Chem. Phys.*, 2013, **15**, 12004–12025.
62 P. M. Oliver, G. W. Watson, E. Toby Kelsey and S. C. Parker, *J. Mater. Chem.*, 1997, **7**, 563–568.
63 N. H. de Leeuw, S. C. Parker, H. M. Sithole and P. E. Ngoepe, *J. Phys. Chem. B*, 2000, **104**, 7969–7976.
64 A. Beltrán, L. Gracia and J. Andrés, *J. Phys. Chem. B*, 2006, **110**, 23417–23423.
65 S. A. Akhade and J. R. Kitchin, *J. Chem. Phys.*, 2012, **137**, 084703.
66 Z. Xu and J. R. Kitchin, *J. Chem. Phys.*, 2015, **142**, 104703.
67 A. J. Hatt, N. A. Spaldin and C. Ederer, *Phys. Rev. B*, 2010, **81**, 054109.

68 H. Guo, K. Chen, Y. Oh, K. Wang, C. Dejoie, S. A. S. Asif, O. L. Warren, Z. W. Shan, J. Wu and A. M. Minor, *Nano Lett.*, 2011, **11**, 3207–3213.

69 S. Cherevko, A. R. Zeradjanin, A. A. Topalov, N. Kulyk, I. Katsounaros and K. J. J. Mayrhofer, *ChemCatChem*, 2014, **6**, 2219–2223.

70 N. Danilovic, R. Subbaraman, K. C. Chang, S. H. Chang, Y. Kang, J. Snyder, A. P. Paulikas, D. Strmcnik, Y. T. Kim, D. Myers, V. R. Stamenkovic and N. M. Markovic, *Angew. Chem. Int. Edit.*, 2014, **53**, 14016–14021.

71 Z. Xu and J. R. Kitchin, *J. Phys. Chem. C*, 2014, **118**, 25597–25602.

72 F. Calle-Vallejo, D. Loffreda, M. T. Koper and P. Sautet, *Nat. Chem.*, 2015, **7**, 403–410.

73 M. Koelsch, S. Cassaignon, J. Guillemoles and J. Jolivet, *Thin Solid Films*, 2002, **403-404**, 312–319.

74 D. Reyes-Coronado, G. Rodríguez-Gattorno, M. E. Espinosa-Pesqueira, C. Cab, R. de Coss and G. Oskam, *Nanotechnology*, 2008, **19**, 145605.

75 J. Choi, H. Park and M. R. Hoffmann, *J. Phys. Chem. C*, 2010, **114**, 783–792.

76 N. B. Halck, V. Petrykin, P. Krtil and J. Rossmeisl, *Phys. Chem. Chem. Phys.*, 2014, **16**, 13682–13688.

77 R. Frydendal, M. Busch, N. B. Halck, E. A. Paoli, P. Krtil, I. Chorkendorff and J. Rossmeisl, *ChemCatChem*, 2015, **7**, 149–154.

78 T. A. Betley, Q. Wu, T. Van Voorhis and D. G. Nocera, *Inorg. Chem.*, 2008, **47**, 1849–1861.

79 M. García-Mota, A. Vojvodic, F. Abild-Pedersen and J. K. Nørskov, *J. Phys. Chem. C*, 2013, **117**, 460–465.